Polish J. of Environ. Stud. Vol. 19, No. 3 (2010), 611-620

Original Research

El Niño's Impact on the Probability Distribution of Sea Level Anomaly Fields

Tomasz Niedzielski[1, 2]*, Wiesław Kosek[1, 3]**

[1]Space Research Centre, Polish Academy of Sciences, Bartycka 18A, 00-716 Warszawa, Poland
[2]Oceanlab, University of Aberdeen, Main Street, Newburgh,
Aberdeenshire AB41 6AA, Scotland, United Kingdom
[3]Environmental Engineering and Land Surveying, University of Agriculture in Kraków,
Balicka 253A, 30-198 Kraków, Poland

Received: 28 September 2009
Accepted: 8 February 2010

Abstract

The sea level anomaly (SLA) gridded time series obtained from TOPEX/Poseidon and Jason-1 satellite altimetry are available from 10.01.1993 to 14.07.2003 with sampling interval of approximately 10 days and spatial resolution of 1° ×1°. It is widely known that the SLA data limited to the equatorial Pacific comprise the El Niño/Southern Oscillation (ENSO) signal. The potential departures from the normal distribution of the SLA data may be due to the ENSO impact and can significantly increase the errors of sea level change predictions in this region.

The objective of this paper is to check if the SLA gridded data for the global ocean being monitored by TOPEX/Poseidon and Jason-1 satellite altimetry follow the normal distribution and to link possible departures from this distribution for the equatorial Pacific with the ENSO events. In order to evaluate this we produced the maps demonstrating the spatial variability of the SLA statistical properties, i.e. trend, standard deviation, skew and kurtosis. In addition, the Shapiro-Wilk test for normality was applied. The assessments were made using the de-trended gridded SLA data, after subtracting or not the model of 365-, 182 and 62-day oscillations. The trend and seasonal oscillations were determined using the least-squares fit. The SLA data in many parts of the global ocean were found to depart from the normal distribution. In particular, the strong departures were distinguished in two zones in the eastern and central-western equatorial Pacific Ocean. The considerable skew in the eastern equatorial Pacific is probably linked to the predominance of El Niño's signal amplitude over La Niña's signal amplitude in the SLA data. The low values of skew for the central-western equatorial Pacific may suggest the opposite relation. The high values of kurtosis are interpreted as evidence of high intermittency of the ENSO signal in the SLA time series in the equatorial Pacific. High values of skew and kurtosis explain possible causes of the SLA prediction errors obtained elsewhere using linear autoregressive technique. The non-linear models are recommended for forecasting sea level change in the equatorial Pacific.

Keywords: sea level anomaly, TOPEX/Poseidon, Jason-1, satellite altimetry, El Niño/Southern Oscillation, normal distribution

*e-mail: niedzielski@cbk.waw.pl
**e-mail: kosek@cbk.waw.pl

Introduction

Sea level change is one of the most current scientific topics. Broadly speaking, it is related to climate change studies and hence it is in the scope of the Intergovernmental Panel of Climate Change (IPCC). Sea level change reveals both temporal and spatial variability. Sea level fluctuations exhibit oscillations with periods ranging from days to centuries. In addition, sea level variations may also vary depending on the ocean region. There are three main groups of processes responsible for sea level fluctuations. The first group comprises eustatic processes that are related to water mass contribution to the ocean. The second group, however, is associated with steric effects which describe the variation of water volume without the change of its mass. Such effects are driven by thermal water fluctuation (thermosteric contribution) and variation dependent on salinity changes (halosteric contribution). The third group of effects consists of geologic and geomorphologic processes acting in the sea floor driving the ocean basins to change their volumes. Apart from this division, it is important to stress the essential role of the El Niño/Southern Oscillation (ENSO) in controlling both regional and global sea level changes. In particular, the impact of ENSO on sea level fluctuations is evident in the equatorial Pacific.

Sea level change is now being monitored by tide-gauges and satellite altimetry. Tide-gauges provide the relative measurements and thus it is tough to distinguish between sea level rise and vertical land movements. In contrast, satellite altimeters can serve well the purpose of obtaining sea surface height (SSH), the value of which is absolute and independent of land motions. There have been many investigations on sea level change based on tide-gauges [1-4] and satellite altimetry [5-8]. The research focused on the estimation of the rate of sea level change [1-4, 6], ocean dynamics studies [5, 7], and sea level prediction [8-10] and modelling [11]. The new era of space-born radar altimetry began in 1978 with the launch of the SEASAT satellite but the biggest step in capturing ocean circulation from space was achieved in 1992 with the launch of the American-French TOPEX/Poseidon satellite [12, 13]. The observations of TOPEX/Poseidon and its successors, Jason-1 [12, 14] and Jason-2 [12], enabled the researchers to compute the spatially dense sea level height measurements (1° ×1°) with the satisfactory sampling interval of approximately 10 days.

The SSH values are computed in respect to the reference ellipsoid. But in order to capture the dynamic ocean topography they can also be expressed as the sea level anomaly (SLA) in respect to the long-term mean sea level. The SLA data comprise a wide range of knowledge about the global ocean dynamics, including the monitoring of extreme sea level fluctuations in the equatorial Pacific during El Niño and La Niña events. The TOPEX/Poseidon altimetry was able to detect large-scale ocean dynamics including the ENSO signal [15]. It has been found from TOPEX/Poseidon measurements that sea level has risen in the eastern equatorial Pacific up to 40 cm during the El Niño 1997/1998 [7] but the annual and semi-annual oscillations have mainly contributed to this rise (34 cm) [8]. The SLA time series determined by modern satellite altimetry and limited to the equatorial regions of the Pacific can be used as the ENSO indicator.

The satellite altimetric time series have been used as input data for calculating ENSO predictions. Among others, Ji et al. [16] assimilated the TOPEX/Poseidon data to the U.S. National Centers for Environmental Prediction (NCEP) ocean global circulation model in order to support ENSO forecasting. Fischer et al. [17] used TOPEX/Poseidon and ERS-1 sea level anomalies and Zheng et al. [18] applied the TOPEX/Poseidon and Jason-1 data to enhance the ensemble ENSO predictions. Niedzielski and Kosek [8, 10] applied the TOPEX/Poseidon and Jason-1 SLA time series to predict sea level fluctuations and the ENSO signal in the SLA data recorded in the vicinity of the eastern equatorial Pacific.

It is now well known that the ENSO signals in many Earth-related data reveal spikes of extreme magnitudes. Such powerful and irregular fluctuations introduce a certain level of non-linearity corresponding to the non-linearity of changes in the surface winds over the tropical Pacific – the main cause of El Niño events [19]. The ENSO-driven spikes are also present in the SLA gridded time series and hence they increase the prediction errors of these data. Many prediction methods, however, are often based on the assumption that the data follow the normal (Gaussian) distribution. In fact, the departure from the normal distribution can introduce the prediction errors. The objective of this paper is to check the normality hypothesis of the SLA time series corresponding to the global ocean being monitored by TOPEX/Poseidon and Jason-1 satellite altimetry. The particular emphasis, however, is put on the equatorial Pacific and the surrounding regions in order to enable ENSO-related inference. The picture of sea level dynamics for the global ocean can be treated as a background for the ENSO studies. A few measures dedicated for testing normality hypothesis are utilized (skewness, kurtosis and the Shapiro-Wilk statistics) and the spatial distributions of their values are presented on maps.

The moment-based tests for the Gaussian distribution of sea surface temperature in the equatorial Pacific and Niño indices were performed by Burgers and Stephenson [20] as well as Hunt and Elliot [21] who related their results to El Niño phenomena. However, there is no similar exercise performed for sea level fluctuations for the global ocean, particularly for the equatorial Pacific. Knowledge about where the probability distribution departs from Gaussian probability law can be essential for improving the SLA and the ENSO predictions.

Data

For the analysis, the gridded SLA time series obtained from the TOPEX/Poseidon and Jason-1 SSH measurements were used. The SLA data were provided by the Center for Space Research, University of Texas at Austin, USA, in the corrected form, i.e. after removal of the following effects:

ocean and pole tides, ionospheric and tropospheric delay of the radar signal, inverse barometer (IB) effect, and electromagnetic bias. The analyzed spatial extent coincides with the TOPEX/Poseidon and Jason-1 maximum coverage that is equivalent to the rectangle 65°S-65°N (latitudes 1-130) and 0°-180°E with 0°-180°W (longitudes 1-360). The available data span the time interval from 10.01.1993 to 14.07.2003 covering the TOPEX/Poseidon satellite cycles No. 12-364 and Jason-1 satellite cycles Nos. 4-56. The missing data were interpolated using the linear interpolation independently for each grid. Due to technical constraints we interpolated (in time) only those data sets that comprise less than or equal to 1% of no data masks. The SLA-gridded data from both satellites were combined using the common observational interval (18 common cycles, i.e. Nos. 347-364 for TOPEX/Poseidon and Nos. 4-21 for Jason-1) and by calculating the relative offset between the two SLA data sets for each grid. The mean offset was added to the Jason-1 SLA data for each grid to calculate the combined SLA data sets.

Prior to the test for normal distribution, the SLA-gridded time series $X(t) = [X_{\lambda,\varphi}(t)]_{\lambda,\varphi \in A}$ spatially limited to the rectangle $A = \{(\lambda,\varphi):\lambda \in [1;360],\ \varphi \in [1;130]\}$ were transformed into two separate data sets:

(1) the de-trended gridded SLA time series $Y(t)$ and
(2) the SLA data after subtracting the model for the trend, annual, semi-annual and 62-day oscillations $Z(t)$.

The power of these harmonic terms significantly varies between remote locations of the global ocean. The annual and semi-annual components are present for almost all locations under study but reveal dissimilar magnitudes. The 62-day term is an alias-type oscillation corresponding to the residual M2 tide in some coastal regions due to unmodelled tidal effects [7, 22-24]. Removal of these deterministic signals can emphasize the ENSO-driven fluctuations, particularly in the equatorial Pacific. The first data set, $Y(t)$, is computed in the following way:

$$Y_{\lambda,\varphi}(t) = X_{\lambda,\varphi}(t) - [B_{\lambda,\varphi}t + \gamma_{\lambda,\varphi}] \tag{1}$$

...where $Y_{\lambda,\varphi}(t)$ corresponds to the value of $Y(t)$ in the grid of location (λ,φ), $X_{\lambda,\varphi}(t)$ is the value of the original time series $X(t)$ in the grid of location (λ,φ) and $[B_{\lambda,\varphi}t + \gamma_{\lambda,\varphi}]$ is the linear trend equation for the location (λ,φ) determined using the least-squares fit. The second data set, $Z(t)$, is determined in a similar way using the following expression:

$$Z_{\lambda,\varphi}(t) = X_{\lambda,\varphi}(t) - [\sum_{i=1}^{3} A_{\lambda,\varphi}^{(i)} \sin(\omega_i t + \phi_{\lambda,\varphi}^{(i)}) + B_{\lambda,\varphi}t + \gamma_{\lambda,\varphi}] \tag{2}$$

...where $Z_{\lambda,\varphi}(t)$ corresponds to the value of $Z(t)$ in the grid of location (λ,φ) and the term in square brackets is the polynomial-harmonic model comprising amplitudes $A_{\lambda,\varphi}^{(1)}$, $A_{\lambda,\varphi}^{(2)}$, $A_{\lambda,\varphi}^{(3)}$ phases $\phi_{\lambda,\varphi}^{(1)}$, $\phi_{\lambda,\varphi}^{(2)}$, $\phi_{\lambda,\varphi}^{(3)}$ and linear trend coefficients $B_{\lambda,\varphi}$, $\gamma_{\lambda,\varphi}$. All of these parameters are also estimated by the least-squares technique. Assuming the TOPEX/Poseidon and Jason-1 cycle of approximately 9.915625 days, the considered oscillations have the following frequencies: $\omega_1=(2\pi)/36.83$, $\omega_2=(2\pi)/18.42$ and $\omega_3=(2\pi)/6.26$.

Methods

The following moments are used to assess the normality of the gridded SLA time series $Y(t)$ and $Z(t)$: standard deviation, skewness and kurtosis [25]. Skew and kurtosis for the location (λ,φ) are defined as:

$$S_{\lambda,\varphi} = \frac{\frac{1}{n}\sum_{i=1}^{n}[H_{\lambda,\varphi}(i) - \overline{H}_{\lambda,\varphi}]^3}{s_{\lambda,\varphi}^3} \tag{3}$$

and

$$K_{\lambda,\varphi} = \frac{\frac{1}{n}\sum_{i=1}^{n}[H_{\lambda,\varphi}(i) - \overline{H}_{\lambda,\varphi}]^4}{s_{\lambda,\varphi}^4} \tag{4}$$

...where $s_{\lambda,\varphi}$ is standard deviation at the grid location (λ,φ). In equations (3) and (4), $H_{\lambda,\varphi}(t)$ is either $Y_{\lambda,\varphi}(t)$ or $Z_{\lambda,\varphi}(t)$ computed by equations (1) or (2), respectively. The term $\overline{H}_{\lambda,\varphi}$ describes the mean value of $H_{\lambda,\varphi}(t)$ for the location (λ,φ) and n is the number of points of a time series. Following Joanes and Gill [26], it should be mentioned that the classical estimators of skew and kurtosis are biased. For normal distribution, skew equals 0 and kurtosis equals 3. Positive values of skew traditionally indicate that the probability density function is skewed to the right. In contrast, the negative skewness corresponds to the left-skewed probability density functions. Traditionally, if kurtosis is greater than 3, the probability density function is more peaked than for normal distribution. On the other hand, if kurtosis is less than 3, the probability density function is flattened in respect to the Gaussian distribution. Although the aforementioned operational usage and interpretation of kurtosis holds, the reader shall be aware that the direct relationship between a given kurtosis value and shape of a probability distribution is not entirely clear [27, 28]. In particular, the above-mentioned simplified interpretation of kurtosis shall be complemented by the information discussed by DeCarlo [29]. These include the understanding of relations between kurtosis and tails (kurtosis is not solely a measure of peakedness) and the interpretation of kurtosis in respect to variance (they do not complement each other). Kurtosis is often applied as a measure of intermittency of the system as used by Sen [30].

In addition, a check for the normal distribution can be done using statistical tests. The Shapiro-Wilk test serves well the purpose of assessing normality of the probability density function [31, 32]. The null hypothesis H_0 reads as follows: the given sample is normally distributed. The alternative hypothesis H_1 says that the sample does not follow the Gaussian distribution. The following test statistics is used for the location (λ,φ):

$$W_{\lambda,\varphi} = \frac{[\sum_{i=1}^{n} a_{\lambda,\varphi}(i) H_{\lambda,\varphi}^{(i)}]^2}{\sum_{i=1}^{n} [H_{\lambda,\varphi}(i) - \overline{H}_{\lambda,\varphi}]^2} \quad (5)$$

...where $H_{\lambda,\varphi}^{(i)}$ is the order statistics for a time series $H_{\lambda,\varphi}(t)$ at location (λ,φ), $a_{\lambda,\varphi}(i)$ is the constant determined using means and covariances of order statistics. In order to visualize the results, the p-values (for details see [25]) are calculated for each grid. Although Shapiro-Wilk detects departures from the normal distributions, it cannot be used to assess the manner of such departures [33]. The Shapiro-Wilk test is said to be relatively powerful among common omnibus tests, both for symmetrical and skewed data [34].

The combined TOPEX/Poseidon and Jason-1 gridded time series comprises 388 data and thus the sample size is big enough to carry out inference based on the aforementioned methods.

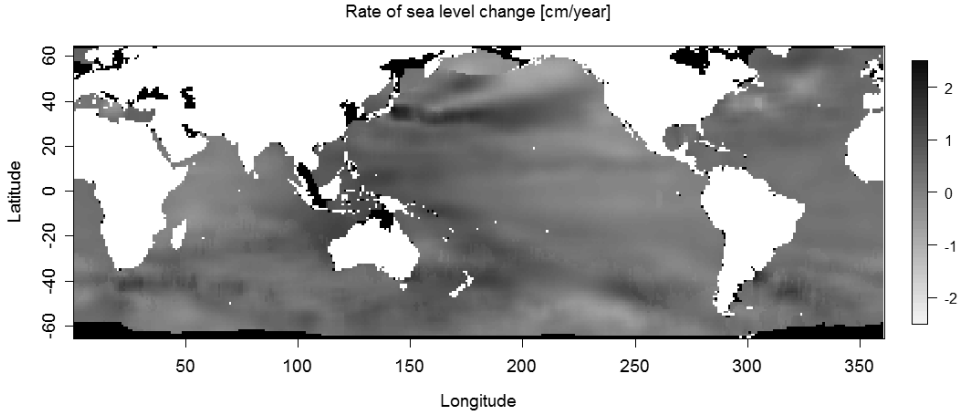

Fig. 1. Rate of sea level change; land is depicted in white; locations with lack of data or poor interpolation are plotted in black.

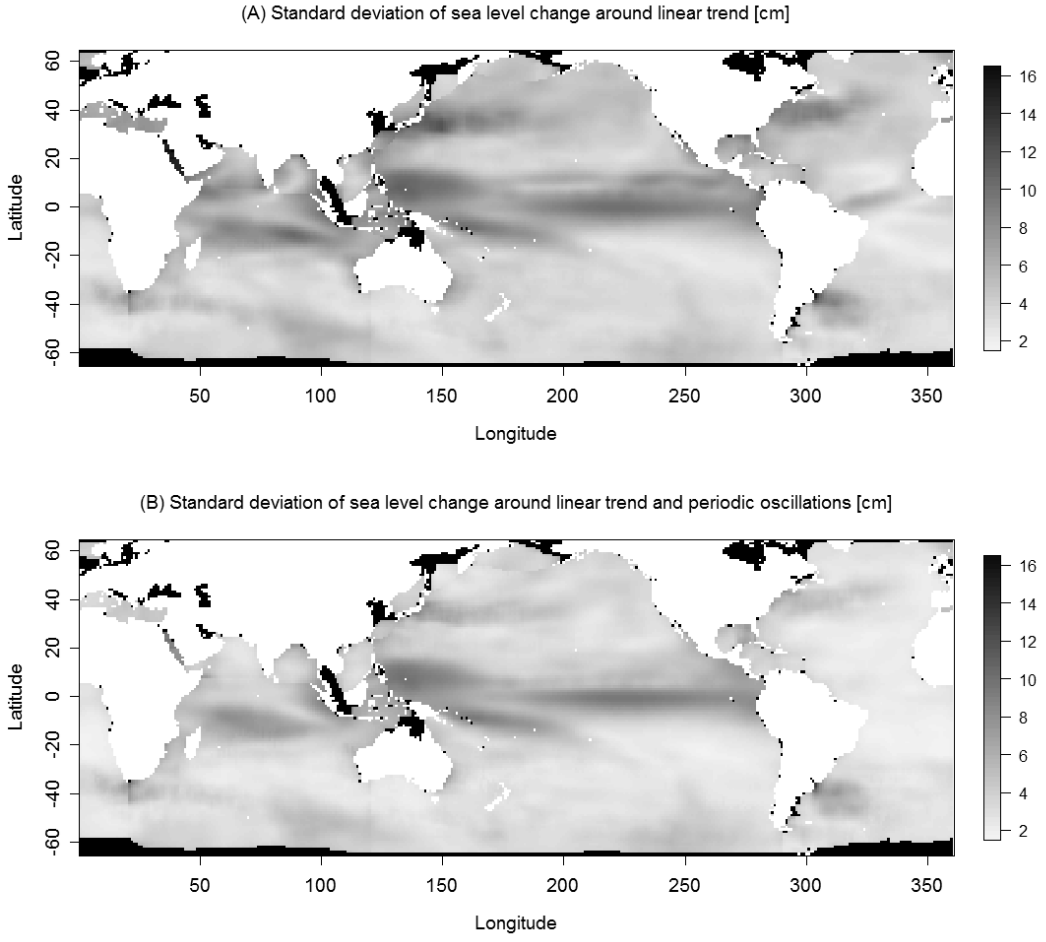

Fig. 2. Standard deviation of the SLA data obtained by removal of: (A) a linear trend, (B) a polynomial-harmonic model comprising a linear trend and oscillations with periods of 365, 182 and 62 days; land is depicted in white; locations with lack of data or poor interpolation are plotted in black.

Results

Fig. 1 demonstrates the rate of sea level change calculated using the least-squares fit for all oceans covered by the TOPEX/Poseidon and Jason-1 observations. In general, the results are in agreement with those obtained earlier by Kosek [7] and Cazenave et al. [35]. The highest sea level rise, exceeding 10 mm/year and locally even 20 mm/year, is noticed for almost the entire west Pacific Ocean, the southeastern Pacific Ocean, the southwestern Atlantic Ocean, the northwestern subarctic Atlantic Ocean, the eastern Indian Ocean and between the Indian and Atlantic oceans (south of the African continent). The strongest decline in sea level, less than -5 mm/year, is detected for the eastern Pacific Ocean from the Equator towards a subarctic zone, the northern Pacific Ocean, the southern Pacific Ocean, the northwestern Atlantic Ocean and the western Indian Ocean. The eastern equatorial Pacific is the region where rates of sea level change vary from a few millimetres below to a few millimetres above zero. These results indicate that even if the eastern equatorial Pacific is prone to extreme sea level rise during El Niño phases, the overall long-term trend in this region fluctuates around zero. The trends demonstrated in Fig. 1 are used to calculate residuals in the subsequent analysis aimed at evaluation of the probability distribution of the SLA data.

Standard deviation of the SLA around a linear trend calculated for all oceans under study varies between 2 to 16 cm (Fig. 2A). The exceptionally high values are recorded in the Red Sea due to big amplitudes of the annual oscillation present in the de-trended signal. The remaining zones of the high standard deviation reaching approximately 10 cm are located in the Pacific Ocean (in the vicinity of the Equator and in the northwestern section of this ocean near Japan), in the central Indian Ocean south of the Equator, in the southwestern and northwestern Atlantic Ocean. Standard deviation around a linear trend in the northern hemisphere is significantly higher than in the southern hemisphere. The same exercise is also performed for the residuals computed by equation (2). The removal of periodic terms results in the reduction of the standard deviation (now from 1.5 to 13.5 cm) because harmonic oscillations do not contribute to the variance of the signal (Fig. 2B). However, the removal of periodic signals does not reduce standard deviation in the equatorial zone of the Pacific. Now, the distinct zone of the highest values is mainly aligned parallel to the Equator. The high standard deviation near the Equator can be linked to the ENSO-driven irregular fluctuations.

Skewness of the SLA residuals computed using equation (1) is approximately between -2.5 and 2.5 and exhibits

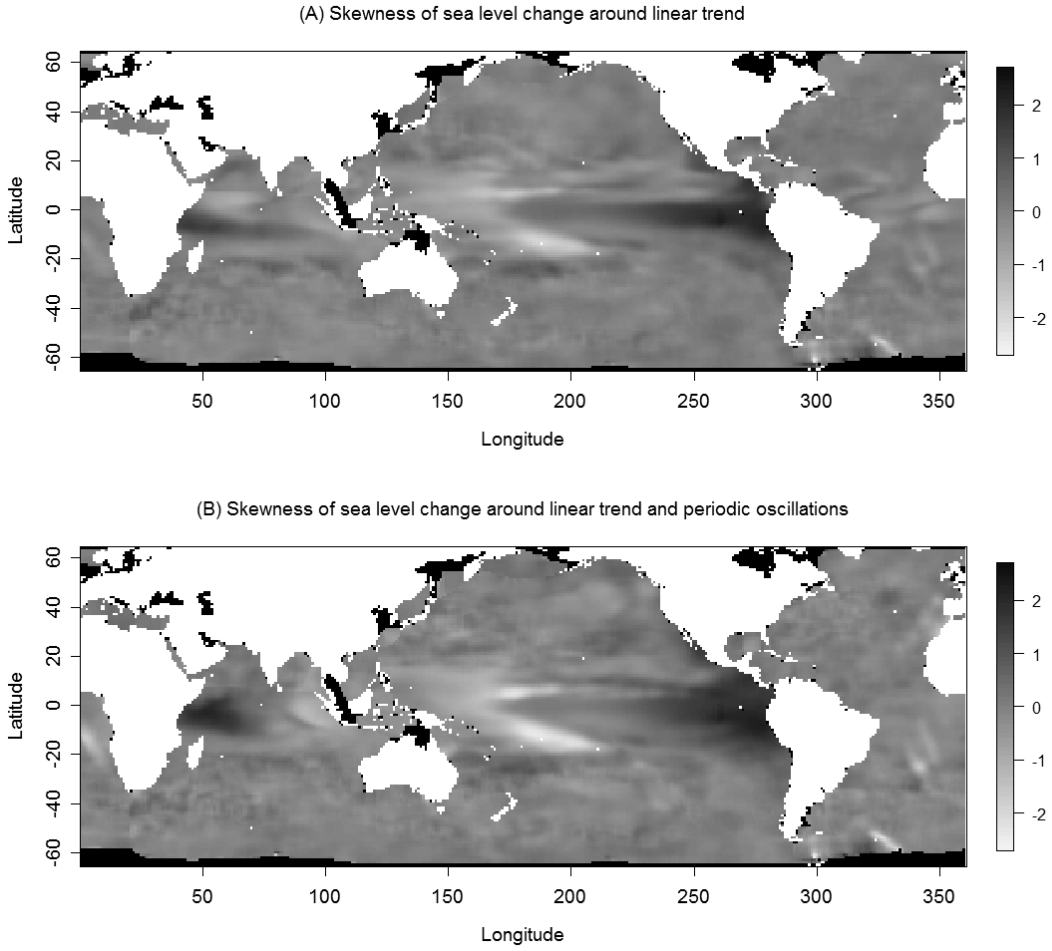

Fig. 3. Skewness of the SLA data obtained by removal of: (A) a linear trend, (B) a polynomial-harmonic model comprising a linear trend and oscillations with periods of 365, 182 and 62 days; land is depicted in white; locations with lack of data or poor interpolation are plotted in black.

the spatial pattern (Fig. 3A). The high values correspond to the eastern equatorial Pacific Ocean (the highest skew) as well as the western equatorial Indian Ocean (considerable skew). In both cases, skew values increase toward land. In addition, the high skew is noticed in the small region in the southwestern Atlantic. These results indicate that the corresponding empirical probability density functions are right-skewed and hence depart from the normal distribution for both aforementioned regions. In contrast, the lowest skew is reported for the centralwestern Pacific at 10°N and 15°S, as well as for the southwestern Atlantic. If the annual, semi-annual and the alias 62-day oscillations are additionally removed from the SLA data using equation (2), the absolute values of skew become slightly higher and reveal the altered spatial distribution (Fig. 3B). Indeed, the eastern equatorial Pacific zone of high skew extends north and south, whereas the western equatorial Indian Ocean zone of the considerable skew becomes more distinct with both higher values of the considered statistics and greater latitudinal spatial extent. Moreover, the zone of low skew in the centralwestern Pacific becomes more evident and reveals further decline in the values of these statistics when the residuals are calculated using equation (2). The same finding holds for the southwestern Atlantic. In addition, if one considers the second-type residuals, it is possible to distinguish the low-skew zones for the southeastern subequatorial Atlantic and the eastern equatorial Indian Ocean. The increase of both, the absolute values of skew and its spatial extent in respect to the results demonstrated in Fig. 3A, can be interpreted as the effect of residual preparation. The residual time series produced using equation (2) are more skewed as they comprise mainly irregular signals, including the ENSO-related extreme sea level fluctuations being relatively rare events. Heavily skewed empirical probability distributions of the SLA residuals observed in the vicinity of the Equator can be link to El Niño and La Niña events, introducing the non-linearity of the sea level variations.

Similar spatial patterns can be observed for kurtosis. Fig. 4A shows kurtosis for residuals calculated by equation (1). The values of kurtosis reveal a considerable spread, from 1.5 to 21.5. The dramatically high values in respect to different ones are reported for the southwestern Atlantic. The highest values of kurtosis there are aligned along the narrow zone, the origin of which is difficult to explain. The intermediate values of the analyzed statistics spatially correspond to the eastern and centralwestern equatorial Pacific. Hence, they are roughly in agreement with zones of high absolute skew values. A more detailed picture for the equa-

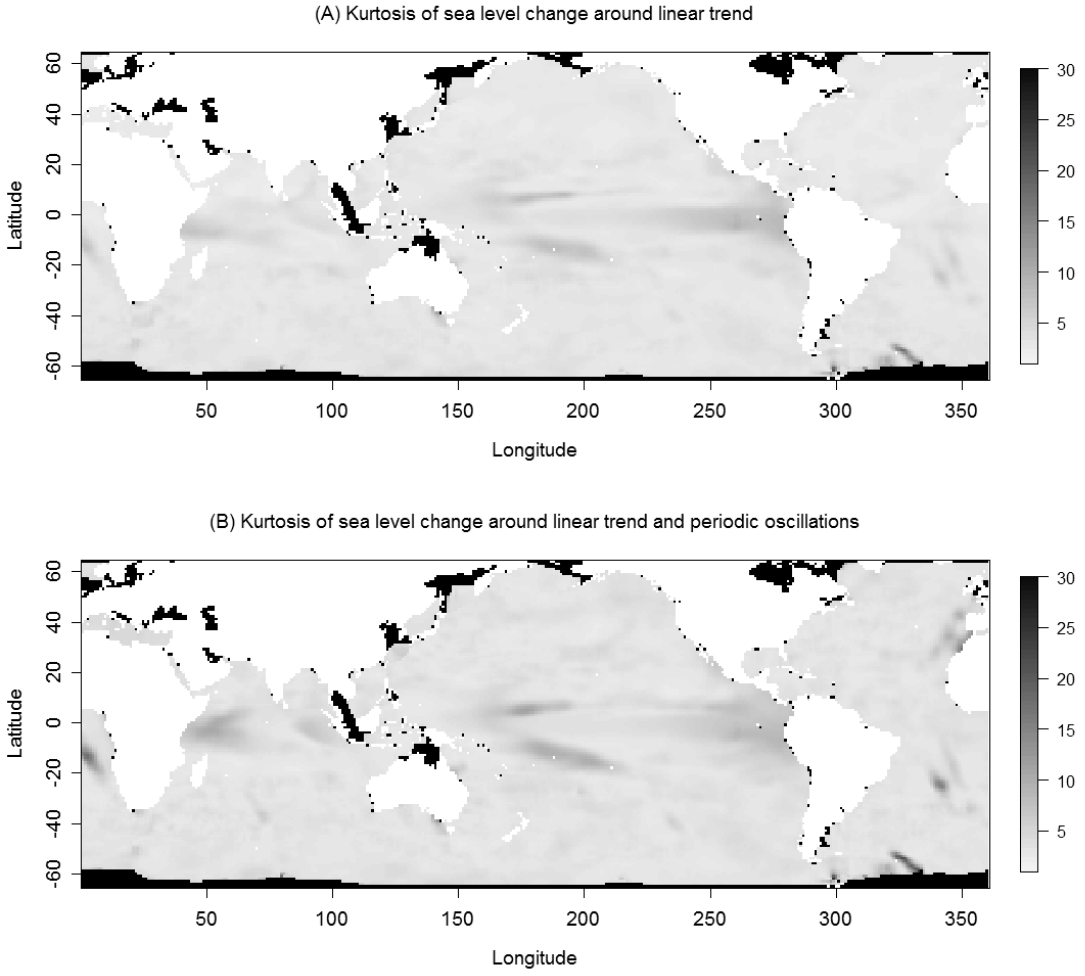

Fig. 4. Kurtosis of the SLA data obtained by removal of: (A) a linear trend, (B) a polynomial-harmonic model comprising a linear trend and oscillations with periods of 365, 182 and 62 days; land is depicted in white; locations with lack of data or poor interpolation are plotted in black.

torial Pacific is depicted in Fig. 5A. In the vicinity of the Equator in the Pacific Ocean, kurtosis varies between 2 and 9. The values of the particularly high kurtosis in Fig. 5A correspond to the eastern and centralwestern equatorial Pacific as reported earlier for skew. In the case of the SLA residuals with periodic oscillations and a trend removed by equation (2), the regions of high kurtosis values (now ranging from 2 to 29 for the global ocean and from 2 to 11 for the equatorial Pacific) have slightly wider spatial extents (Figs. 4B and 5B). This finding can also be interpreted as the effect of residual calculation. In addition, a few zones of intermediate kurtosis are detectable using residuals calculated by equation (2), i.e. in the western equatorial Indian Ocean as well as in the southeastern subequatorial Atlantic. The results indicate that in this ENSO-vulnerable region the empirical probability density functions are more peaked than the Gaussian distribution. This finding, together with the above-mentioned high skew reported for this region, classifies the probability distribution as a heavy-tailed one. The results can be interpreted using the notion of intermittency which is detectable by the high kurtosis. The intermittent time series comprises bursts of activity (El Niño or La Niña events) and stable periods (ENSO normal conditions). The regions with the high kurtosis correspond to the intermittent zones due to the ENSO impact.

In order to confirm the above-mentioned results based on the interpretations of skew and kurtosis, the Shapiro-Wilk test for normal distribution is performed independently for the residuals calculated using equations (1) and (2). The results are depicted in Fig. 6. In almost the entire equatorial and subequatorial zone, the Shapiro-Wilk test rejects the normality hypothesis. The regions where the SLA residual are normally distributed are patchy and prevail in the southern hemisphere. As a result of the application of the Shapiro-Wilk test, sea level observed in the equatorial Pacific with the concurrent high skew and kurtosis can definitely be assumed to be non-Gaussian, heavy-tailed and intermittent.

Conclusions

The sea level anomalies in many parts of the global ocean depart from normal probability distribution. This finding is particularly strong if one considers specific zones in the equatorial Pacific Ocean. Indeed, the equatorial zones

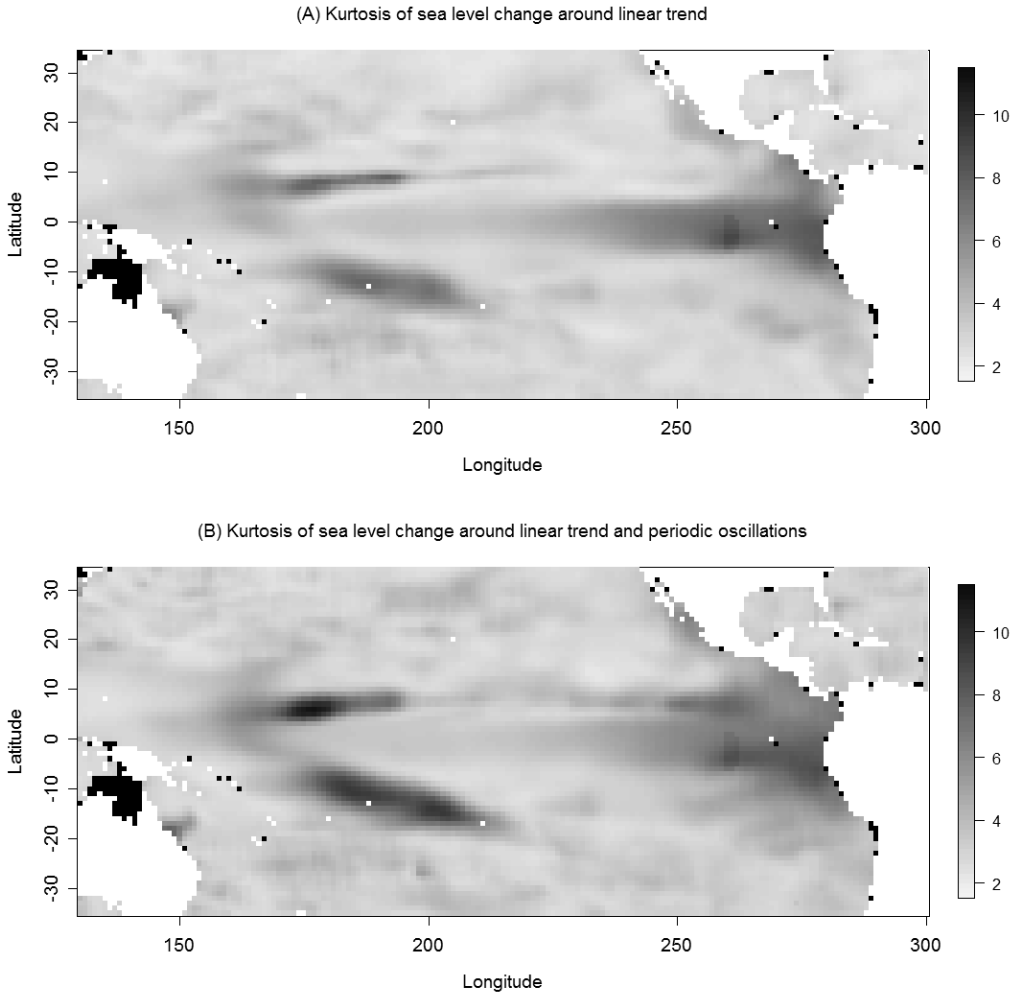

Fig. 5. Kurtosis of the SLA data for the equatorial Pacific obtained by removal of: (A) a linear trend, (B) a polynomial-harmonic model comprising a linear trend and oscillations with periods of 365, 182 and 62 days; land is depicted in white; locations with lack of data or poor interpolation are plotted in black.

located in the eastern and centralwestern Pacific are characterized by the relatively high skew (implying the heavy right-tail of the empirical probability density function) and high kurtosis (corresponding to the intermittency of the local sea level change). The positively skewed probability distribution indicates that the extremely high values prevail over the extremely low untypical values. In the context of the ENSO studies this means that El Niño events are much more evident in the eastern equatorial Pacific than La Niña episodes. This finding coincides with the results by Burgers and Stephenson [20] who found the predominance of El Niño signal over La Niña signal in the sea surface temperature for this region. In contrast, the negatively skewed probability distribution suggests that very low values prevail over very high numbers. In the context of the results obtained for the centralwestern equatorial Pacific. In the context of the results obtained for the central-west equatorial Pacific, this may also mean the predominance of El Niño signal over La Niña signal, however, due to local sea level decline in this area.

On the other hand, the positive kurtosis implies the considerable intermittency of the system. In particular, the sea level anomalies in the eastern and the centralwestern equatorial Pacific comprise rather short bursts of high activity (El Niño or La Niña) interrupted by rather long periods of quiet (normal conditions). In the case of the ENSO investigations, the intermittency of large amplitude sea surface temperature anomalies in Niño 3.4 region (5°S to 5°N, 170°W to 120°W) has also been reported by Hunt and Elliot [21]. The magnitude of right heavy-tail property and intermittency in the investigated sea level anomalies for the eastern equatorial Pacific becomes lower if the distance from the Equator increases. In contrast, the significant left heavy-tail property and intermittency in the centralwestern Pacific Ocean is reported for 10°N and 15°S, hence not at zero-latitude.

Following Burgers and Stephenson [20], we argue that knowledge about the departures of sea level anomalies from normality can support the ENSO prediction studies. Skew and kurtosis are the measures of non-linearity of the system and hence may help in the model selection studies. Indeed, the atmospheric response to El Niño and La Niña is perceived to be non-linear [36] and hence local sea level fluctuations due to the ENSO can also be assumed to be far from linear. High values of skew and kurtosis reported in this paper explain the causes of sea level anomalies' prediction errors obtained using the linear autoregressive technique by Niedzielski and Kosek [8]. Indeed, the models

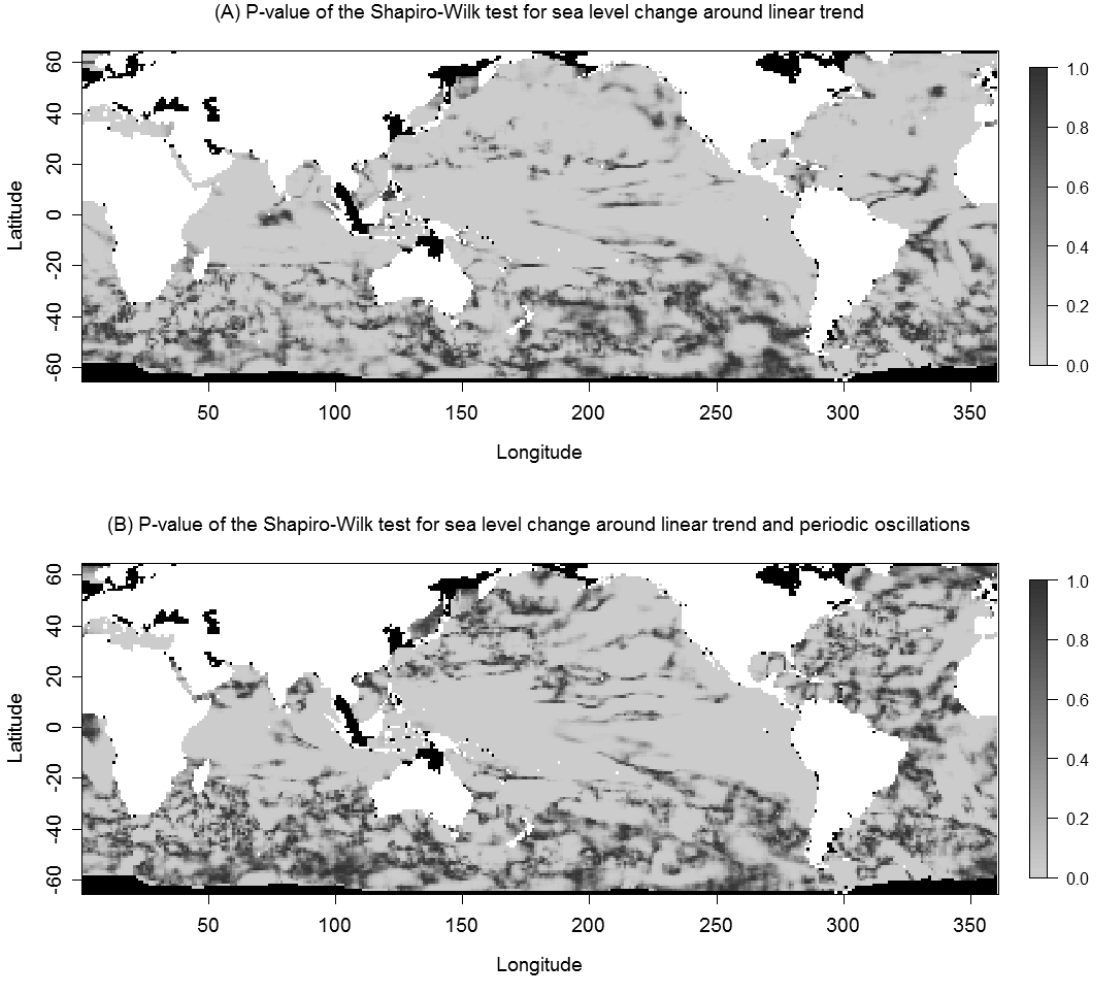

Fig. 6. P-value of the Shapiro-Wilk test for the SLA data obtained by removal of: (A) a linear trend, (B) a polynomial-harmonic model comprising a linear trend and oscillations with periods of 365, 182 and 62 days; land is depicted in white; locations with lack of data or poor interpolation are plotted in black.

with zero skew tend to underestimate the high quantiles (El Niño) which are detected by the high skew computed from the data [20]. Thus, the non-linear models would be recommended for forecasting sea level change in the equatorial Pacific, particularly in the selected zones distinguished in this study.

Acknowledgements

Our research was financed by Polish science funds for 2009-10 provided by the Polish Ministry of Science and Higher Education through grant No. N N526 160136 under the leadership of Dr. Tomasz Niedzielski at the Space Research Centre of the Polish Academy of Sciences. The first author is also supported by the EU EuroSITES project. The authors thank the Center for Space Research, University of Texas at Austin, USA, for providing the TOPEX/Poseidon and Jason-1 data. The authors of R 2.9.0 - A Language and Environment and additional packages are acknowledged. Last but not least we are grateful to the anonymous referee for insightful comments that led to the improvement of this paper.

References

1. GORNITZ V., LEBEDEFF S. Global sea-level changes during the past century. In: NUMMEDAL A. et al. (eds) Sea-level fluctuation and coastal evolution. Society of Economic Paleontologists and Mineralogists Special Publication **41**, 3, **1987**.
2. DOUGLAS B.C. Global sea level rise. Journal of Geophysical Research **96**, 6981, **1991**.
3. UNAL Y.S., GHIL M. Interannual and interdecadal oscillation patterns in sea level. Climate Dynamics **11**, 255, **1995**.
4. DOUGLAS B.C. Sea level change in the era of the recording tide gauge. In: DOUGLAS B.C., KEARNEY M.S., LEATHERMAN S.P. (Eds) Sea level rise: history and consequences. Academic Press, San Diego, pp. 37-64, **2001**.
5. NEREM R.S., SCHRAMA E.J., KOBYLINSKY C.J., BECKLEY B.D. A preliminary evaluation of ocean topography from the TOPEX/POSEIDON mission. Journal of Geophysical Research **99**, (C12), 24565, **1994**.
6. LEULIETTE E.W., NEREM R.S., MITCHUM G.T. Calibration of TOPEX/Poseidon and Jason altimeter data to construct a continuous record of mean sea level change. Marine Geodesy **27**, 79, **2004**.
7. KOSEK W. Long-term and short period global sea level changes from TOPEX/Poseidon altimetry. Artificial Satellites **36**, 71, **2001**.
8. NIEDZIELSKI T., KOSEK W. Forecasting sea level anomalies from TOPEX/Poseidon and Jason-1 satellite altimetry. Journal of Geodesy **83**, 469, **2009**.
9. RÖSKE F. Sea level forecasts using neural networks. Ocean dynamics **49**, 71, **1997**.
10. NIEDZIELSKI T., KOSEK W. Multivariate stochastic prediction of the global mean sea level anomalies based on TOPEX/Poseidon satellite altimetry. Artificial Satellites **40**, 185, **2005**.
11. BARBOSA S.M., SILVA M.E., FERNANDES M.J. Multivariate autoregressive modelling of sea level time series from TOPEX/Poseidon satellite altimetry. Nonlinear Processes in Geophysics **13**, 177, **2006**.
12. CAZENAVE A., LOMBARD A., LLOVEL W. Present-day sea level rise: a synthesis. Comptes Rendus Geosciences **340**, 761, **2008**.
13. FU L.-L., CHRISTENSEN E.J., YAMARONE C.A. JR., LEFEBVRE M., MÉNARD Y., DORRER M., ESCUDIER P. TOPEX/POSEIDON mission overview. Journal of Geophysical Research **99**, (C12), 24369, **1994**.
14. LAFON T. JASON 1: lessons learned from the development and 1 year in orbit. Acta Acta Astronautica **56**, 45, **2005**.
15. NEREM R.S., CHAMBERS D.P., LEULIETTE E.W., MITCHUM G.T., GIESE B.S. Variations in global mean sea level associated with the 1997-98 ENSO event: implications for measuring long term sea level change. Geophysical Research Letters **26**, 3005, **1999**.
16. JI M., REYNOLDS R.W., BEHRINGER D.W. Use of TOPEX/Poseidon Sea Level Data for Ocean Analyses and ENSO Prediction: Some Early Results. Journal of Climate **13**, 219, **2000**.
17. FISCHER M., LATIF M., FLÜGEL M., JI M. The Impact of Data Assimilation on ENSO Simulations and Predictions. Monthly Weather Review **125**, 819, **1997**.
18. ZHENG F, ZHU J., ZHANG R.-H. Impact of altimetry data on ENSO ensemble initializations and predictions, Geophysical Research Letters 34, L13611, doi:10.1029/2007GL030451, **2007**.
19. PHILANDER S.G. El Niño, La Niña, and the Southern Oscillation. Academic Press, San Diego, pp. 293, **1990**.
20. BURGERS G., STEPHENSON D.B. The "Normality" of El Niño. Geophysical Research Letters **26**, (8), 1027, **1999**.
21. HUNT B.G., ELLIOT T.I. Secular variability of ENSO events in a 1000-year climatic simulation. Climate Dynamics **20**, 689, **2003**.
22. WAGNER C.A., TAI C.K., KUHN J.M. Improved M2 ocean tide from TOPEX/POSEIDON and Geosat Altimetry. Journal of Geophysical Research **99**, (C12), 24853, **1994**.
23. KATZ E.J., BUSALACCHI A., BUSCHNELL M., GONZALES F., GOURDEAU L., McPHADEN M., PICAUT J. A comparison of coincidental time scales of the ocean surface height by satellite altimeter, mooring and inverted echo sounder. Journal of Geophysical Research **100**, (C12), 25101, **1995**.
24. CHERNIAWSKY J.Y., FOREMAN M.G.G, CRAWFORD W.R., HENRY R.F. Ocean Tides from TOPEX/Poseidon Sea Level Data. Journal of Atmospheric and Oceanic Technology **18**, 649, **2001**.
25. ROGERSON P.A. Statistical Methods for Geography. A student's guide. SAGE, pp. 304 **2006**.
26. JOANES D.N., GILL C.A. Comparing measures of sample skewness and kurtosis. The Statistician **47**, 183, **1998**.
27. BALANDA K.P., MacGILLYVRAY H.L. Kurtosis: A Critical Review. The American Statistician **42**, 111, **1988**.
28. BALANDA K.P., MacGILLYVRAY H.L. Kurtosis and spread. The Canadian Journal of Statistics **18**, 17, **1990**.
29. DeCARLO L.T. On the Meaning and Use of Kurtosis. Psychological Methods **2**, 292, **1997**.
30. SEN A.K. Spectral-temporal characterization of riverflow variability in England and Wales for the period 1865-2002. Hydrological Processes **23**, 1147, **2009**.
31. SHAPIRO S.S., WILK M.B. An analysis of variance test for normality (complete samples). Biometrika **52**, 591, **1965**.

32. ROYSTON P. A Remark on Algorithm AS 181: The W Test for Normality. Applied Statistics **44**, 547, **1995**.
33. BROWN B.M., HETTMANSPERG T.P. Normal Scores, Normal Plots, and Tests for Normality. Journal of American Statistical Association **91**, 1668, **1996**.
34. PEARSON E.S., D'AGOSTINO R.B., BOWMAN K.O. Tests for departure from normality: Comparison of powers. Biometrika **64**, 231, **1977**.
35. CAZENAVE A., CABANES C., DOMINH K., GENNERO M.C., LE PROVOST C. Present-Day Sea Level Change: Observations and Causes. Space Science Reviews **108**, (1-2), 131, **2003**.
36. HOERLING M.P., KUMAR A., ZHONG M. El Niño, La Niña, and the Nonlinearity of Their Teleconnections. Journal of Climate **10**, 1769, **1997**.